Electromagnetic Modeling of Moving Mixed Conductive and Dielectric BoRs with an Effective Domain Decomposition Method

Electromagnetic Modeling of Moving Mixed Conductive and Dielectric BoRs with an Effective Domain Decomposition Method

Mengmeng Li, *Senior Member*, *IEEE*, Yanmeng Hu, Rushan Chen, *Senior Member*, *IEEE*, and Giuseppe Vecchi, *Fellow*, *IEEE*

***Abstract*—We propose an effective domain decomposition method with spherical equivalence surface for the electromagnetic modeling and imaging of moving bodies of revolution (BoRs) from near coupling to far coupling region. The moving BoRs are modeled with a series of stationary moments with respect to the time, each object is enclosed by a spherical equivalence surface. In the near coupling region, the couplings between multiple BoRs are evaluated with the couplings between spherical equivalence surfaces. While in the far coupling region, the total scattering fields are obtained by the superposition of the scattering fields from each spherical equivalence surface. For the moving objects with different relative positions at stationary moments, the equivalence processes are evaluated only once with combined field integral equation (CFIE) and Poggio-Miller-Chang-Harrington-Wu-Tsai (PMCHWT) equations for conductive and dielectric objects, respectively. The radar images are obtained from the scattering electromagnetic fields evaluated by the proposed domain decomposition method. Both computation accuracy and efficiency are enhanced significantly. Numerical results and discussions demonstrate the validity of the proposed method for modeling and imaging of mixed conductive and dielectric multiple moving objects.**

***Index Terms*—Multiple moving objects, near coupling, radar imaging, equivalence**

I. INTRODUCTION

ELECTROMAGNETIC modeling and imaging of moving multiple objects are important topics in computational electromagnetic (CEM). Aside from theoretical interest, this finds practical application in several aerospace-related situations, typically in the tracking of payloads or sub-vehicles after separation from the rocket module in the fairing phase. Current high-end application, both in civil and defense rocketry, call for *multiple* orbiting mission payloads. In this phase, flight is essentially ballistic. The reference situation then is one with multiple objects, moving independently in ballistic flight; both conductive and dielectric targets are usually present in the same launch group. Along their trajectory, they pass gradually from the initial situation of strong electromagnetic coupling region (due to proximity) to the far weak coupling region. Effective modeling and electromagnetic simulation of this process is very important for radar imaging and identification.

To model the electromagnetic properties of high-speed moving objects, the finite difference time domain (FDTD) method with relative boundary condition was introduced to evaluate the scattering field from moving boundaries [1]. Improvements of the relativistic boundary conditions were introduced in FDTD for the modeling of transient responses of moving objects [2]. The Lorentz-FDTD was introduced to transform the incident plane wave to a moving coordinate system for the modeling of high speed moving dielectric objects [3], [4]. The time domain integral equation (TDIE) method [5], [6] based on relativistic space-time transformation and electromagnetic transformation was proposed for the modeling of transient responses by an accelerated or arbitrarily moving objects [7], [8].

The error from electromagnetic quasi-stationary approximation for moving objects is on the order of v/c, where v is the maximum speed of moving boundary and c is the speed of light in vacuum [9]. As a result, for the multiple targets with speeds much smaller than c discussed in this work, they can be evaluated with a series of stationary moments with respect to the time. Modeling of a single moving object could be substituted as a stationary problem with multiple incident directions, i.e. multiple right-hand vectors of the matrix equation. Many techniques for instance interpolation/extrapolation [10]-[12], asymptotic waveform evaluation [13], [14], model based parameter estimation [15], fast direct inversion method [16]-[21], and other relative wideband/wide-angle acceleration methods [22], [23] can be employed to solve this problem. For single moving targets but with precession motion, the dynamic far fields can be extracted from the table of static far fields obtained by measurements or simulations [24].

This work was supported in part by Natural Science Foundation of China of 61890540, 61890541, and 61871222, in part by the Natural Science Foundation of Jiangsu Province under Grant BK20171429, in part by the Fundamental Research Funds for the Central Universities under Grant 30918011103, in part by the Postgraduate Research & Practice Innovation Program of Jiangsu Province under Grant SJCX19_0063.

M. Li, Y. Hu, and R. S. Chen are with the Department of Communication Engineering, Nanjing University of Science and Technology, Nanjing, China (e-mail: limengmeng@njust.edu.cn; eerschen@njust.edu.cn).

G. Vecchi is with the Antenna and EMC Laboratory (LACE), Politecnico di Torino, 10125 Turin, Italy (e-mail: giuseppe.vecchi@polito.it).

For the modeling of multiple moving objects, in which the relative positions of the objects are varying with the time, the stationary simulation is not a simple matrix equation with multiple right-hand vectors. The impedance matrix would be changed with respect to the varying relative positions among the multiple objects, as a result, at each sampling time state, the impedance matrix would be evaluated repeatedly. Many fast integral solvers of multilevel fast multipole algorithm (MLFMA) [25], FFT-based method [26]-[28], low rank matrix compression method [29]-[33], and macro basis function method [34], [35] could be employed to accelerate the modeling of the multiple objects with different relative positions. The tailored MLFMA was introduced for the modeling of multiple moving targets in a large space distributions with discretized stationary moments [36], [37].

Recently, we introduced the equivalence principle algorithm (EPA) [38], [39] to the multiple BoRs with arbitrary oriented axes [41], where the spherical equivalence surface was used to enclose each BoR, then the couplings between two BoRs with different oriented axes can be substituted with the coupling of two spherical equivalence surfaces a common oriented axis. For multiple BoRs with different axes, the standard BoR method of moments (MoM-BoR) formulation results in a dense coupling impedance matrix which leads to high computation complexity [40], [41]. Instead, when evaluating the couplings between individual BoRs via the corresponding spherical equivalence surfaces, a common axis can be employed, resulting in a block diagonal matrix, with the corresponding drastic reduction in computation complexity [41]. Further, we extended it for the simulation of multiscale problems [42] and aircraft arrays [43]. Similar interesting work in [44] with domain decomposition method was proposed for stationary mixed metallic-dielectric BoRs.

In this work, the multiple mixed dielectric and conductive BoRs moving from near (strong) coupling region to far (weak) coupling region are simulated with discretized stationary moments [36], [37]. The couplings of multiple BoRs in the near region would be evaluated with couplings between equivalence surfaces. While in the far region, the total scattering field can be obtained by the superposition of the scattering field from each equivalence surface. For the stationary objects with different relative positions during the moving process, the equivalence processes are evaluated only once with combined field integral equation (CFIE) [45], [46] and Poggio-Miller-Chang-Harrington-Wu-Tsai (PMCHWT) [47]-[49] equations for conductive and dielectric problems, respectively. The radar image is extracted from the electromagnetic scattering fields, much weaker scattering fields from the dielectric objects can be found with respect to the conductive ones. With the proposed method, the electromagnetic simulations of the multiple mixed dielectric and conductive BoRs during the whole moving process are evaluated accurately and effectively. It paves a way for further moving multiple targets imaging and identification.

The remainder of the paper is organized as follows: in Section II, a detailed description of the algorithm is proposed; numerical results and discussions in Section III demonstrate the validity of the proposed method. Finally, a brief conclusion is given in Section IV.

II. Theory

In this section, detailed theory for the modeling of moving multiple BoRs with arbitrary oriented axes is proposed, the multiple BoRs can be conductive, dielectric, or mixed conductive and dielectric.

A. Domain Decomposition Method (DDM) for the Modeling of Moving Multiple BoRs

Fig. 1 shows a stationary moment for two cones separated from the cylindrical body. The rotation axis of target t_1 is z_1, the rotation axis of target t_2 is z_2, and the rotation axis of target t_3 is z_3. t_1 and t_3 are conductive objects, t_2 is dielectric target. All these three BoRs are with different rotation axes, the MoM-BoR cannot be employed effectively [40], [41]. For our proposed domain decomposition method, the spherical equivalence surfaces (ES_1 to ES_3) are introduced to enclose each target, then for t_1 and t_2, the corresponding equivalence surfaces ES_1 and ES_2 would share a common rotation axis z, as a result, the coupling between t_1 and t_2 can be evaluated with MoM-BoR effectively [41]-[43].

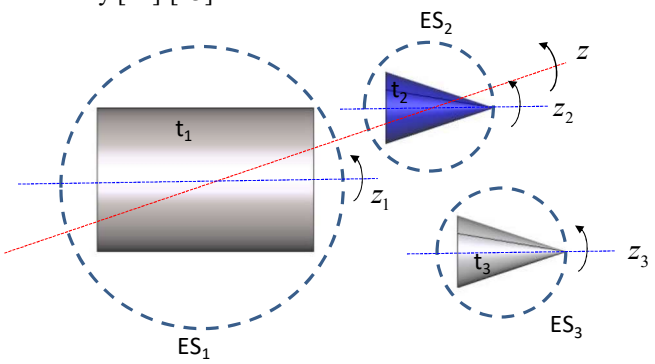

Fig. 1 Modeling of two cones when separating from the cylindrical body at a stationary moment. These three BoRs are denoted as t_1 with rotation axis z_1, t_2 with rotation axis z_2, and t_3 with rotation axis z_3. t_1 and t_3 are conductive objects, t_2 is dielectric target. The whole problem is decomposed into three subdomains, each subdomain is enclosed with spherical equivalence surface denoted as ES_1, ES_2, and ES_3, respectively.

As shown in Fig.1, without loss of generality, for the target denoted as i_{th} subdomain, when considering the mutual coupling with other subdomains, the scattering current densities $\left[\mathbf{j}_i^{sca}\ \mathbf{m}_i^{sca}\right]^{\mathrm{T}}$ of i_{th} subdomain can be expressed as [41]-[43]

$$\begin{bmatrix} \mathbf{j}_i^{sca} \\ \frac{1}{\eta}\mathbf{m}_i^{sca} \end{bmatrix} = \mathbf{S}_i \begin{bmatrix} \mathbf{j}_i^{inc} \\ \frac{1}{\eta}\mathbf{m}_i^{inc} \end{bmatrix} + \mathbf{S}_i \left(\sum_{j=1, j\neq i}^{Q} \mathbf{T}_{ij} \begin{bmatrix} \mathbf{j}_j^{sca} \\ \frac{1}{\eta}\mathbf{m}_j^{sca} \end{bmatrix} \right) \tag{1}$$

The two terms of the right-hand of Eq. (1) are due to the incident currents $\left[\mathbf{j}_i^{inc}\ \mathbf{m}_i^{inc}\right]^{\mathrm{T}}$ and the scattering currents from all other subdomains $\left[\mathbf{j}_j^{sca}\ \mathbf{m}_j^{sca}\right]^{\mathrm{T}}$, respectively. Matrix $\mathbf{S}_i$ is the

scattering operator of the i_{th} subdomain describing the relationship between the incident currents to the scattering currents, matrix $\mathbf{T}_{ij}$ is the translation operator describing the couplings of equivalence surfaces from j_{th} to i_{th} subdomain. The scattering operator is defined as

$$\mathbf{S}_i = \left[\mathbf{Z}_i^{hp}\right]\left[\mathbf{Z}_i^{pp}\right]^{-1}\left[\mathbf{Z}_i^{ph}\right] \tag{2a}$$

$$\left[\mathbf{Z}_i^{hp}\right] = \begin{bmatrix} -\hat{n}\times\mathbf{K} & \frac{1}{\eta}\hat{n}\times\mathbf{L} \\ -\frac{1}{\eta}\hat{n}\times\mathbf{L} & -\hat{n}\times\mathbf{K} \end{bmatrix} \tag{2b}$$

$$\left[\mathbf{Z}_i^{pp}\right] = \begin{bmatrix} \mathbf{L}+\mathbf{L}_1 & \eta\mathbf{K}+\eta_1\mathbf{K}_1 \\ -(\eta\mathbf{K}+\eta_1\mathbf{K}_1) & \mathbf{L}+\mathbf{L}_1 \end{bmatrix} \tag{2c}$$

$$\left[\mathbf{Z}_i^{ph}\right] = \begin{bmatrix} -\mathbf{L} & -\eta\mathbf{K} \\ \eta\mathbf{K} & -\mathbf{L} \end{bmatrix} \tag{2d}$$

where the superscript *h* and *p* denote the surfaces of equivalence spheres and target t_i, $\hat{n}$ denotes the outside normal vector on the target t_i. η and η_1 are the wave impedance for the free space and material in the region of the object t_i. $\mathbf{L}$ and $\mathbf{K}$ are the electric and magnetic integral operators as defined in [38], [42], where the subscript 1 in Eq. (2c) denotes operator for the internal region unknowns of the PMCHWT [47]-[50] for homogenous dielectric target t_i, when for conductive problems, this term would be zero, the operator in Eq. (2c) is simplified as the expression in [43].

The translation operator between the equivalence surfaces [41]-[43] is defined as

$$\mathbf{T}_{ij} = \begin{bmatrix} -\hat{n}\times\mathbf{K} & \frac{1}{\eta}\hat{n}\times\mathbf{L} \\ -\frac{1}{\eta}\hat{n}\times\mathbf{L} & -\hat{n}\times\mathbf{K} \end{bmatrix}. \tag{3}$$

When the couplings between two BoRs (i_{th} and j_{th} subdomains) are evaluated with MoM-BoR, transformations and rotations are required for three defined local coordinate systems (x_i, y_i, z_i), (x_i', y_i', z_i'), and $(x_{ij}'', y_{ij}'', z_{ij}'')$. The local coordinate system (x_i, y_i, z_i) is parallel with the global coordinate, the local coordinate system (x_i', y_i', z_i') coincides with the axis of the enclosed BoR objects, and the local coordinate system $(x_{ij}'', y_{ij}'', z_{ij}'')$ coincides with the axis shared by two coupling spherical equivalence surfaces. With the rotation matrices, the currents on equivalence surfaces between two local coordinates can be transformed with

$$\mathbf{j}_i = \mathbf{R}_i^1 \mathbf{j}_i' \tag{4a}$$

$$\mathbf{j}_i = \mathbf{R}_{ij}^2 \mathbf{j}_i'' \tag{4b}$$

$\mathbf{R}_i^1$ is the rotation matrix transform the current $\mathbf{j}_i'$ in coordinate system (x_i', y_i', z_i') to the current $\mathbf{j}_i$ in coordinate system of (x_i, y_i, z_i), $\mathbf{R}_{ij}^2$ is the rotation matrix transform the current $\mathbf{j}_i''$ in coordinate system $(x_{ij}'', y_{ij}'', z_{ij}'')$ to the current $\mathbf{j}_i$ in coordinate system of (x_i, y_i, z_i). For a reference point in the coordinate system of either (x_i', y_i', z_i') or $(x_{ij}'', y_{ij}'', z_{ij}'')$, its coordinate is (x_r, y_r, z_r) in the coordinate system (x_i, y_i, z_i), the rotation pitching and azimuth angle θ_r and φ_r [41], [42] are determined as

$$\theta_r = \arccos\left(\frac{z_r}{\sqrt{x_r^2+y_r^2+z_r^2}}\right) \tag{5}$$

$$\varphi_r = \arctan\left(\frac{y_r}{x_r}\right) \tag{6}$$

with the rotation angle, the transformation and rotation matrices between two coordinate systems defined on the BoRs, spherical equivalence surface, and two coupling spherical equivalence surfaces can be obtained as derived in [41], [42]. Finlay, Eq. (1) is derived with the coordinate transformation

$$\begin{aligned} \begin{bmatrix} \mathbf{j}_i^{sca} \\ \frac{1}{\eta}\mathbf{m}_i^{sca} \end{bmatrix} = \mathbf{R}_i^1\mathbf{S}_i\tilde{\mathbf{R}}_i^1 \begin{bmatrix} \mathbf{j}_i^{inc} \\ \frac{1}{\eta}\mathbf{m}_i^{inc} \end{bmatrix} + \\ \mathbf{R}_i^1\mathbf{S}_i\tilde{\mathbf{R}}_i^1 \left(\sum_{j=1, j\neq i}^{Q} \mathbf{R}_{ij}^2\mathbf{T}_{ij}\tilde{\mathbf{R}}_{ij}^2 \begin{bmatrix} \mathbf{j}_j^{sca} \\ \frac{1}{\eta}\mathbf{m}_j^{sca} \end{bmatrix} \right) \end{aligned} \tag{7}$$

$\tilde{\mathbf{R}}_i^1$ and $\tilde{\mathbf{R}}_{ij}^2$ are the rotation matrices [41], [42] transform the current $\mathbf{j}_i$ in coordinate system (x_i, y_i, z_i) to the current $\mathbf{j}_i'$ in the coordinate system of (x_i', y_i', z_i') and $\mathbf{j}_i''$ in the coordinate system of $(x_{ij}'', y_{ij}'', z_{ij}'')$, respectively.

B. Accelerations of DDM for the Modeling of Moving Multiple BoRs

Further accelerations are employed to enhance the proposed EPA-BoR-DDM for multiple moving objects. When the moving time is discretized with a series of stationary moments, the relative positions among multiple objects are changed and the computation domain is enlarged [36], [37]. In our proposed DDM with spherical equivalence surfaces, as in Eq. (7), only the evaluation of the rotation matrices $\mathbf{R}_i^1$, $\tilde{\mathbf{R}}_i^1$, $\mathbf{R}_{ij}^2$, $\tilde{\mathbf{R}}_{ij}^2$ and translation operators $\mathbf{T}_{ij}$ between two spherical equivalence surfaces are required repeatedly with a low computation cost. As a result, the evaluations of moving multiple objects are simplified as iterations with Eq. (7) with pre-computed rotation matrices, translation operators, and single-times evaluated scattering operators.

Besides, the translators between two spherical equivalence surfaces are demonstrated to be low-rank matrices [51], recently developed low-rank matrix compression methods [31]-[33] can

be employed to sparse the translation matrix as

$$\mathbf{T}_{ij} = \mathbf{U}_{ij}\mathbf{D}_{ij}\mathbf{V}_{ij} \tag{8}$$

$\mathbf{U}_{ij}$, $\mathbf{D}_{ij}$, and $\mathbf{V}_{ij}$ are the receiving, translation, and radiation matrices obtained from a nested equivalence source approximation [31]-[33].

III. NUMERICAL RESULTS AND DISCUSSION

In this section, numerical simulations are presented to validate the accuracy and efficiency of the proposed scheme. All the computations have been carried out serially on the same computer with an Intel (R) Core (TM) i7-8700 CPU @3.7GHz, 64 GB of RAM.

A. Modeling of the Multiple BoRs with Near Couplings

First, the bistatic RCS of two separated targets are simulated as in Fig. 2, the conductive cylinder is with diameter 1 m and height 3 m, the dielectric cone ($\varepsilon_r = 2.0, \mu_r = 1.0$) is with diameter 1 m and height 3 m. The distances between them in $\hat{z}$ and $\hat{y}$ directions are 0.5 m. The incident plane wave is from $(\theta = 0^\circ, \phi = 0^\circ)$, the observation angle is from 0° to 360°, the simulated frequency is at 3 GHz. As shown in Fig. 3, a very good agreement can be found with respect to MLFMA in commercial software FEKO [52], which demonstrates the accuracy of the proposed method.

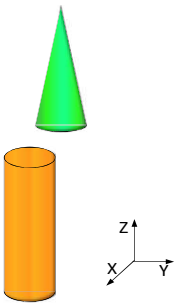

Fig. 2 Schematic diagram of two separated targets. The conductive cylinder is with diameter 1 m and height 3 m, the dielectric cone ($\varepsilon_r = 2.0, \mu_r = 1.0$) is with diameter 1 m, and height 3 m.

The radar image of two separated targets shown in Fig. 2 are simulated, the incident plane wave frequencies are within $f \in [2.7\text{GHz}, 3.3\text{GHz}]$, the incident directions are within $\theta \in [-4^\circ, 4^\circ]$, and the resolutions in range and azimuth directions are 0.25 m and 0.35m, respectively. As shown in Fig. 4, the position of the strong scattering point on the bottom edge of the conductive cylinder appears at the range distance of 3m and the azimuth distance is from -0.5 m to 0.5 m. The position of the strong scattering point on the dielectric cone appears at the range distance of 0.5m and the azimuth distance is from 0.5 m to 1.0 m. The distributions of strong scattering points are consistent with the actual relative positions in Fig. 2. Compared with the conductive cylinder, the amplitudes of the scattering fields from the dielectric cone are much weaker.

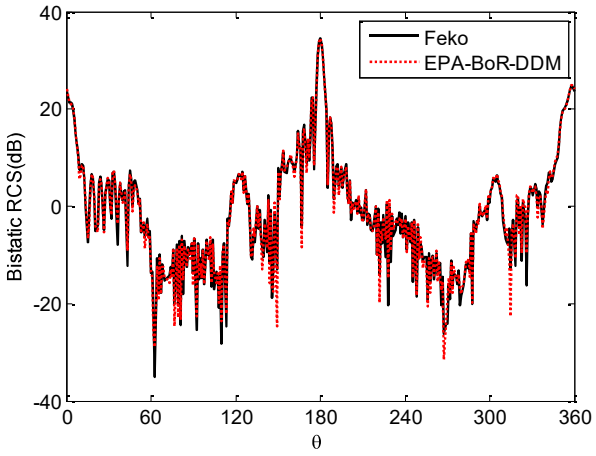

Fig. 3 Validation: simulation of bistatic RCS for two separated targets with proposed EPA-BoR-DDM and MLFMA in FEKO [52]. The incident plane wave at 3 GHz is from $(\theta = 0^\circ, \phi = 0^\circ)$, and the observation angle is from 0° to 360°.

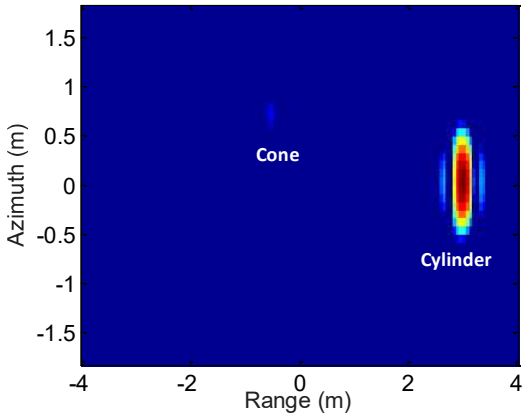

Fig. 4 Simulated radar image of the near coupling conductive cylinder and dielectric cone.

B. Modeling of Separating Multiple BoRs

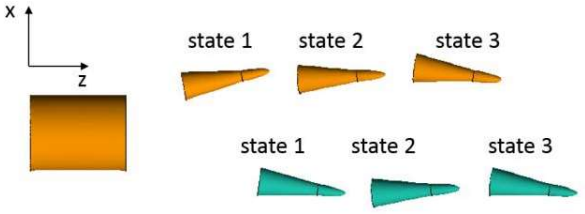

Fig. 5 Two targets separating from the cylindrical body, states 1 to 3 are three modeling stationary moments. The radius and height of the targets are 0.075 m and 0.46 m, the radius and height of the body are 0.2 m and 0.5 m, the precession motion angle and period along the axis are 10° and 1 s, respectively.

In this part, the realistic multiple moving targets at a series of stationary moments are simulated. As shown in Fig. 5, two targets are separating from the conductive cylindrical body. The top one is conductive and the bottom one is dielectric ($\varepsilon_r = 2.0, \mu_r = 1.0$). The radius and height of the target are

0.075 m and 0.46 m, the radius and height of the body are 0.2 m and 0.5 m. The incident plane wave at 3 GHz is from $(\theta=0^\circ,\phi=0^\circ)$, the observation angle is from 0° to 180°. As shown in Fig. 5, state 1 is the initial stationary moment of the targets, states 2 and 3 are the stationary moments after 0.2 s and 0.4 s, respectively. The conductive and dielectric targets have different relative separating velocities, meanwhile, during the separating process, the precession motion angle and period of the targets along the axis are 10° and 1 s, respectively.

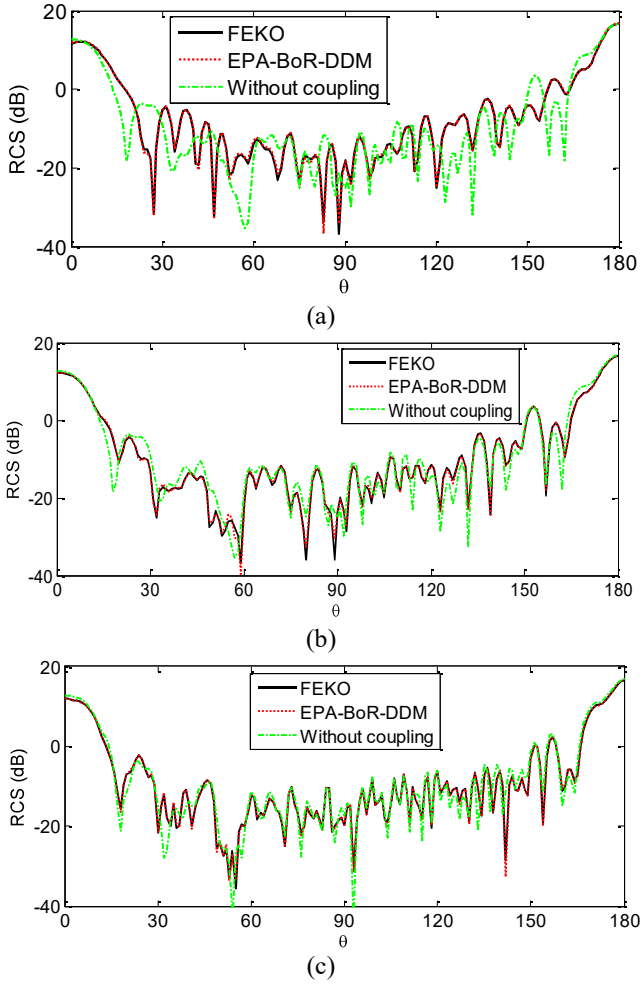

Fig. 6 Simulated bistatic RCS at (a) state 1, (b) state 2, and (c) state 3 of the separating targets when considering the near couplings with FEKO, proposed EPA-BoR-DDM, and the method without considering the couplings. The incident plane wave at 3 GHz is from $(\theta=0^\circ,\phi=0^\circ)$, the observation angle is from 0° to 180°.

The proposed EPA-BoR-DDM is used to simulate the separating targets at state 1 to 3, excellent agreements of the simulated bistatic RCS with respect to the results from MLFMA in FEKO [52] are shown in Fig. 6 (a) to (c). The results of the simulation without considering near couplings are obtained by solving each target separately and adding the scattering fields directly [36]. Obvious differences between the results with and without near coupling in the near region are found as shown in Fig. 6 (a) and Fig. 6 (b). With the increase of separating distances between the three targets, the effects from the near coupling can be neglected as in Fig. 6 (c). As a result, the total RCS can be obtained by the superposition of scattering fields from the equivalence surfaces directly in the far region.

At the initial stationary moment of state 1, the generatrix of three spherical equivalence surfaces are divided into 762 segments for the proposed EPA-BoR-DDM, the total simulation time and memory requirements are 163 MB and 30 s, while for the MLFMA, 10144 number of triangle patches are employed for the surface discretization, the total simulation time and memory requirements are 635 MB and 180 s. Significant computation efficiency enhancement is achieved. Furthermore, in our simulation of moving targets, we evaluate the equivalence operator only once at the initial state, during the separating process, only the coordinate rotation matrices are required to be evaluated and stored. As a result, our proposed method paves an effective way for the modeling of multiple moving objects.

C. *Modeling of Moving BoRs Along Designed Tracks*

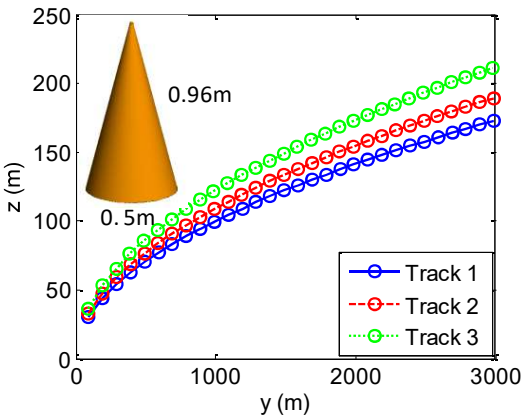

Fig. 7 Designed tracks of three moving cones with precession motions, the functions of the curves are $y_1=1/10z_1^2$, $y_2=1/12z_2^2$, and $y_3=1/12z_3^2$. The conductive cones are moving along tracks 1 and 2, while the dielectric cone is moving along track 3.

Table I Precession motions parameters of the three cones, θ_c and θ_d are the precession angle of the conductive and dielectric cones, respectively.

states	conductive targets		dielectric target	
	precession period T (s)	precession angle θ_c	precession period T (s)	precession angle θ_d
1	-	0	-	0
2	4	5°	4	8°
3	4	8°	4	11°
4	4	10°	4	13°

Fig. 7 shows the designed three tracks of two conductive cones and one dielectric cone, where track 1 and 2 are for conductive cones, track 3 is for dielectric cone with $\varepsilon_r=2.0$. The diameters and heights of the cones are 0.5 m and 0.95 m, the

incident plane wave at 1 GHz is from $(\theta = 0^\circ, \phi = 0^\circ)$. The speeds of the cones are 100 m/s, the precession motion parameters are listed as in Table I. Four series of precession motion parameters are designed. The simulated monostatic RCS is plotted in Fig. 8, obvious fluctuations of the RCS curves are found with the increase of procession angles. The characteristics of the RCS for the clusters of the cones with precession motions are very important for potential cognition.

At the start of the moving process $t = 1$s, the generatrix of three spherical equivalence surfaces are divided into 125 segments for the proposed EPA-BoR-DDM, the related time and memory requirements are 12 s and 90 MB, while for the MLFMA in FEKO, 10844 number of triangle patches are employed for the surface discretization, the time and memory requirements are 280 s and 1.9 GB, respectively. For a series of simulations of moving cones at 30 stationary moments, much better computation performance would be achieved due to the strategies described in Sec. II-B.

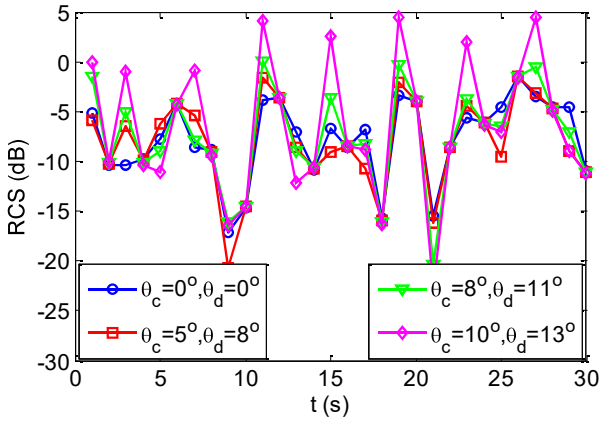

Fig. 8 Monostatic RCS of the three cones at 1 GHz moving along the designed tracks with a speed of 100 m/s, respectively, the precession motion parameters are listed as in Table I.

Fig. 9 (a) shows the radar image of the three cones at t = 1 s, the centroid coordinates of them are (0, 92.5, 30.4), (0, 91.3, 33.1), and (0, 89.6, 36.7). The incident frequencies are within $f \in [0.5\text{GHz}, 1.5\text{GHz}]$ with the frequency step of 12.5MHz, the incident directions are within $\theta \in [-5^\circ, 5^\circ]$ with the angular step of 0.5°. As shown in Fig.11 (a), the relative range distance between conductive cone 1 and conductive cone 2 is 2.8 m, the relative range distance between conductive cone 2 and dielectric cone 3 is 4.0 m, and the azimuth distance between them are 0 m. The simulated results agree well with the realistic positions. In addition, the scattering fields from the dielectric cone 3 is much weaker than the ones from the conductive cones, which is useful to distinguish it from the mixed conductive and dielectric targets. Similarly, Fig. 9 (b) shows the image when t = 5 s, the centroid coordinates of the cones are (0, 490.4, 70.0), (0, 488.7, 76.6), and (0, 486.4, 85.4). The incident frequencies are within $f \in [0.5\text{GHz}, 1.5\text{GHz}]$ with the frequency step of 6.25 MHz, the incident directions are within $\theta \in [-5^\circ, 5^\circ]$ with the angular step of 0.5°. Similar as the results at t = 1 s in Fig. 9 (a), the simulated results agree well with the realistic positions.

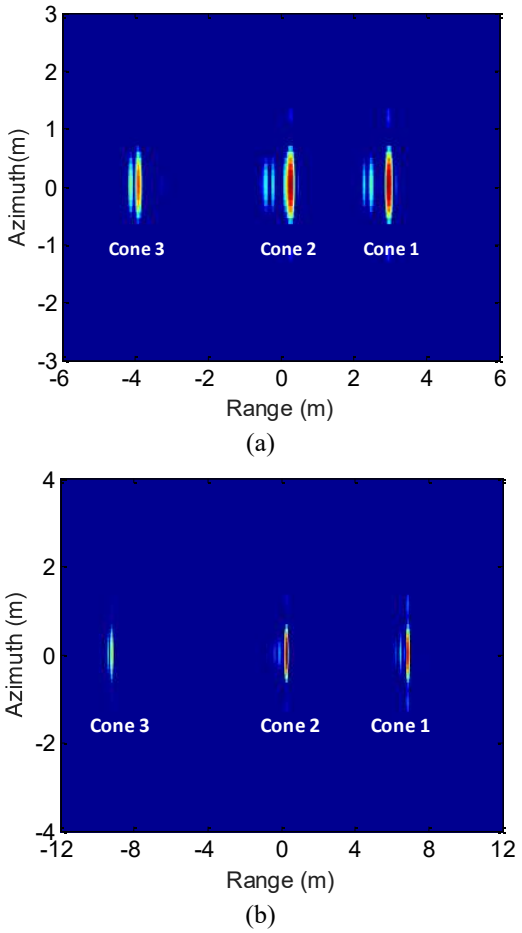

Fig. 9 Simulated radar images for the three moving cones along designed tracks when at (a) t = 1 s and (b) t = 5 s.

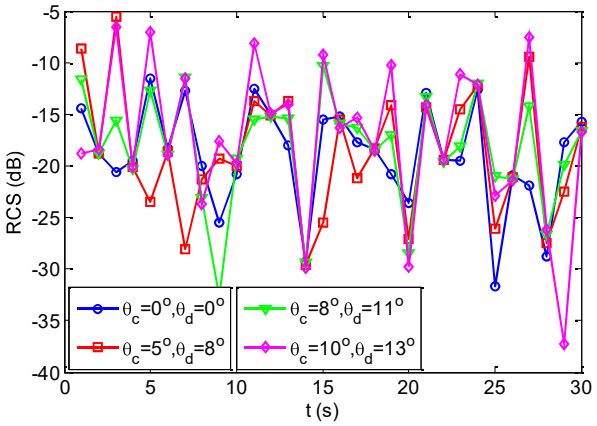

Fig. 10 Monostatic RCS of the three cones at 10 GHz moving along the designed tracks with a speed of 100 m/s, respectively, the precession motion parameters are listed as in Table I.

Fig. 10 shows the monostatic RCS of the three cones in Fig. 7 with the same precession motion parameters and plane wave incident directions, but at the frequency of 10 GHz. Similar as the results at 1 GHz, obvious fluctuations of the RCS curves are found with the increase of procession angles. At the start of the

moving process $t = 1$ s, for the proposed EPA-BoR-DDM, the generatrix of three spherical equivalence surfaces are divided into 1254 segments, the total simulation time and memory requirements are 31 minutes and 7.5 GB, while for the MLFMA, 1.1 million number of triangle patches are employed for the surface discretization, the iterative convergence cannot be achieved due to the ill conditioning performance of PMCHWT matrix equation [47]-[49], [55].

IV CONCLUSION

In this paper, an effective domain decomposition method with spherical equivalence surface for multiple moving mixed dielectric and conductive BoRs is proposed. The multiple moving targets are modeled with a series of stationary moments with respect to the time. For both the conductive and dielectric targets, the equivalence processes which project the currents on the targets to the spherical equivalence surfaces are evaluated only once with surface integral equations. And then, the couplings between two BoR targets with arbitrary oriented axes can be evaluated with MoM-BoR with specific coordinate rotations. A series of realistic multiple moving BoRs are simulated from near to far coupling region, the radar images of the targets are shown to demonstrate the validity of our proposed method.

The simulations of multipole BoRs in this work are limited to the situations in which the equivalence surfaces do not intersect. In cases where this happens, two existing methods [53], [54] can be employed within the present approach, respectively.

REFERENCES

[1] F. Harfoush, A. Taflove, and G. A. Kriegsmann, "A numerical technique for analyzing electromagnetic wave scattering from moving surfaces in one and two dimensions," *IEEE Trans. Antennas Propag.*, vol. 37, no. 1, pp. 55–63, Jan. 1989.

[2] L. Kuang, S. Zhu, J. Gao, Z. Zheng, and D. Dong, "A numerical method for analyzing electromagnetic scattering properties of a moving conducting object," *Int. J. Antennas Propag.*, vol. 2014, Art. no. 386315, 2014

[3] K. Zheng, J.-Z. Li, G. Wei, and J.-D. Xu, "Analysis of Doppler effect of moving conducting surfaces with Lorentz-FDTD method," *J. Electromagn. Waves Appl.*, vol. 27, no. 2, pp. 149–159, Nov. 2013.

[4] K. Zheng, Z. Mu, H. Mu, and G. Wei, "Electromagnetic properties from moving dielectric in high speed with Lorentz-FDTD," *IEEE Antennas Wireless Propag. Lett.*, vol. 15, pp. 934–937, 2016.

[5] Y. Shi, M. Y. Xia, and R. S. Chen, E. Michielssen, M. Lu, "Stable electric field TDIE solvers via quasi-exact evaluation of MOT matrix elements," *IEEE Trans. Antennas Propag.*, vol. 59, 2, pp. 574-585, Dec. 2010.

[6] H. H. Zhang, Z. H. Fan, and R. S. Chen, "Marching-on-in-degree solver of time-domain finite element-boundary integral method for transient electromagnetic analysis," *IEEE Trans. Antennas Propag.*, vol. 62, no. 1, pp. 319-326, Jan. 2013.

[7] S. Q. Jia, X. M. Jiang, and M. Y. Xia, "Numerical approach for analysis of transient scattering by an accelerated body," *J. Electromagn. Waves Appl*., vol. 26, nos. 5–6, pp. 770–782, 2012.

[8] S. Q. Jia and M. Y. Xia, "Numerical simulation of electromagnetic scattering by moving objects based on relativity," *Acta Scientiarum Naturalium Univ. Pekinensis*, vol. 49, no. 6, pp. 1111–1117, Nov. 2013.

[9] J. Cooper, "Scattering of electromagnetic fields by a moving boundary: the one-dimensional case," *IEEE Trans. Antennas Propag.*, vol. 28, no. 6, pp. 791-795, Jun. 1980.

[10] Z. Liu, R.S. Chen, and J. Chen, "Adaptive sampling cubic-spline interpolation method for efficient calculation of monostatic RCS," *Microwave and Optical Technology Letters*, vol.50, no.3, pp.751-755, Mar. 2008.

[11] Z. Liu, D. Z. Ding, Z. H. Fan, and R. S. Chen, "Adaptive sampling bicubic spline interpolation method for fast computation of monstatic RCS," *Microwave and Optical Technology Letters*, vol.50, no.7, pp.1851-1857, Jul. 2008.

[12] J. Yang, T. K. Sarkar, "Interpolation/extrapolation of radar cross-section (RCS) data in the frequency domain using the Cauchy method," *IEEE Trans. Antennas Propag.*, vol. 55, no. 10, pp. 2844-2851, 2007.

[13] C. J. Reddy, M. D. Deshpande, C. R. Cockrell, F. B. Beck, "Fast RCS computation over a frequency band using method of moments in conjunction with asymptotic waveform evaluation technique," *IEEE Trans. Antennas Propag.*, vol. 46, no. 8, pp. 1229-1233, Aug. 1998.

[14] X. C. Wei, Y. J. Zhang, and E. P. Li, "The hybridization of fast multipole method with asymptotic waveform evaluation for the fast monostatic RCS computation," *IEEE Trans. Antennas Propag.*, vol. 52, no. 2, pp. 605–607, Feb. 2004.

[15] E. K. Miller, "Model-based parameter estimation in electromagnetics. I. background and theoretical development," *IEEE Antennas and Propagation Magazine*, vol. 40, no. 1, pp. 42-52, Feb. 1998.

[16] A. Heldring, J. M. Rius, J. M. Tamayo, J. Parrón, and E. Ubeda, "Multiscale compressed block decomposition for fast direct solution of method of moments linear system," *IEEE Trans. Antennas Propag.*, vol. 59, no. 2, pp. 526-536, Dec. 2010.

[17] T. Wan, Z. N. Jiang, and Y. Sheng, "Hierarchical matrix techniques based on matrix decomposition algorithm for the fast analysis of planar layered structures," *IEEE Trans. Antennas Propag.*, vol. 59, no. 11, pp. 4132-4141, Nov. 2011.

[18] J.-G. Wei, Z. Peng, and J.-F. Lee, "A fast direct matrix solver for surface integral equation methods for electromagnetic wave scattering from non-penetrable targets," *Radio Sci*., vol. 47, p. RS5003, 2012.

[19] K. C. Wang, M. Li, D. Z. Ding, R. S. Chen, "A parallelizable direct solution of integral equation methods for electromagnetic analysis," *Engineering Analysis with Boundary Elements*, vol. 85, pp. 158-164, Dec. 2017.

[20] M. Jiang, Z. Rong, L. Lei, X.J Li, Y.P. Chen, S. Sun, Z.P. Nie, and J. Hu, "SIE-DDM based on a hybrid direct-iterative approach for analysis of multiscale problems," *IEEE Trans. Antennas Propag*., vol. 67, no. 12, pp. 7440-7451, Dec. 2019.

[21] Z. Rong, M. Jiang, Y. P. Chen, L. Lei, Z. P. Nie, and J. Hu, "fast Direct surface integral equation solution for electromagnetic scattering analysis with skeletonization factorization," *IEEE Trans. Antennas Propag*., DOI: 10.1109/TAP.2019.2952014, 2020.

[22] X.-M. Pan and X.-Q. Sheng, "Fast solution of linear systems with many right-hand sides based on skeletonization," *IEEE Antennas Wireless Propag. Lett.*, vol. 15, no. 1, pp. 301–304, 2016.

[23] X.-M. Pan, S.-L. Huang, and X.-Q. Sheng, "Wide angular sweeping of dynamic electromagnetic responses from large targets by MPI parallel skeletonization," *IEEE Trans. Antennas Propag.*, vol. 66, no. 3, pp. 1619–1623, Mar. 2018.

[24] L. Liu, P. Zhong, X Li, C. Dai, H. Huang, and Y. Li, "Research on dynamic RCS characteristics of ballistic missile with micro-motion," in *2017 IEEE 2nd International Conference on Signal and Image Processing*, pp. 10-14, Aug. 2017.

[25] J. Song, C. Lu, and W. Chew, "Multilevel fast multipole algorithm for electromagnetic scattering by large complex objects," *IEEE Trans. Antennas Propag*., vol. 45, no. 10, pp. 1488–1493, Oct. 1997.

[26] E. Bleszynski, M. Bleszynski, and T. Jaroszewicz, "AIM: Adaptive integral method for solving large-scale electromagnetic scattering and radiation problems," *Radio Sci*., vol. 31, no. 5, pp. 1225–1251, May 1996.

[27] C. H. Chan and L. Tsang, "A sparse-matrix canonical-grid method for scattering by many scatterers," *Microw. Opt. Technol. Lett*., vol. 8, no. 2, pp. 114–118, Feb. 1995.

[28] S. M. Seo and J. -F. Lee, "A fast IE-FFT algorithm for solving PEC scattering problems," *IEEE Trans. Magn*., vol. 41, pp. 1476–1479, May 2005.

[29] K. Zhao, M. N. Vouvakis, and J.-F. Lee, "The adaptive cross approximation algorithm for accelerated method of moments computations of EMC problems," *IEEE Trans. Electromagn. Compat*., vol. 47, no. 4, pp. 763–773, Nov. 2005.

[30] E. Michielssen and A. Boag, "A multilevel matrix decomposition algorithm for analyzing scattering from large structures," IEEE Trans. Antennas Propag., vol. 44, no. 8, pp. 1086–1093, Aug. 1996
[31] M. Li, M. A. Francavilla, F. Vipiana, G. Vecchi, and R. S. Chen, "Nested equivalent source approximation for the modeling of multiscale structures," *IEEE Trans. Antennas Propag*., vol. 62, no. 7, pp. 3664–3678, Jul. 2014
[32] M. Li, M. A. Francavilla, R. S. Chen, and G. Vecchi, "Wideband fast kernel-independent modeling of large multiscale structures via nested equivalent source approximation," *IEEE Trans. Antennas Propag*., vol.63. no.5, pp.2122-2134, May 2015
[33] M. Li, M. A. Francavilla, D. Z. Ding, R. S. Chen, and G. Vecchi, "Mixed-form nested approximation for wideband multiscale simulations" *IEEE Trans. Antennas Propag*., vol. 66, no. 11, pp. 6128-6136, Nov. 2018
[34] L. Matekovits, V. A. Laza, G. Vecchi, "Analysis of large complex structures with the synthetic-functions approach," *IEEE Trans. Antennas Propag*., vol. 55, no. 9, pp. 2509-2521, Sep. 2007
[35] J. Hu, Y.-K. Li, Z. Nie, and H. Zhao, "Modal characteristic basis function method for solving scattering from multiple conducting bodies of revolution," *IEEE Trans. Antennas Propag.*, vol. 62, no. 2, pp. 870–877, Feb. 2014.
[36] H. L. Zhang, Y. X. Sha, X. Y. Guo, M. Y. Xia, and C. H. Chan, "Efficient analysis of scattering by multiple moving objects using a tailored MLFMA," *IEEE Trans. Antennas Propag.*, vol. 67, no. 3, pp. 2023-2027, Mar. 2019.
[37] H. L. Zhang, Y. X. Sha, X. Y. He, X. Y. Guo, and M. Y. Xia, "Efficient algorithm for scattering by a large cluster of moving objects," *IEEE Access*, vol. 7, pp. 124948-124955, 2019.
[38] M.-K. Li and W. C. Chew, "A domain decomposition scheme based on equivalence theorem," *Microwave Opt. Technol. Lett.*, vol. 48, pp. 1853–1857, Sep. 2006.
[39] M.-K. Li and W. C. Chew, "Multiscale simulation of complex structures using equivalence principle algorithm with high-order field point sampling scheme," *IEEE Trans. Antennas Propag*., vol. 56, no. 8, pp. 2389–2397, Aug. 2008.
[40] W. C. Gibson, *The Method of Moments in Electromagnetics*. London, U.K.: Chapman & Hall/CRC, 2008.
[41] T. Su, L. Du, and R. Chen, "Electromagnetic scattering for multiple PEC bodies of revolution using equivalence principle algorithm," *IEEE Trans. Antennas Propag*., vol. 62, no. 5, pp. 2736–2744, May 2014.
[42] M. Li, T. Su, and R. S. Chen, "Equivalence principle algorithm with body of revolution equivalence surface for the modeling of large multiscale structures," *IEEE Trans. Antennas Propag*., vol. 64, no. 5, pp.1818-1828, May 2016
[43] T. Su, M. Li, and R. S. Chen, "Domain decomposition scheme with equivalence spheres for the analysis of aircraft arrays in a large-scale range," *Engineering Analysis with Boundary Elements*, vol. 73, pp. 42–49, Dec. 2016
[44] M. Jiang, Y. Li, Z. Rong, L. Lei, Y. Chen, and J. Hu, "Fast solving scattering from multiple bodies of revolution with arbitrarily metallic-dielectric combinations," *IEEE Trans. Antennas Propag*., vol. 67, no. 7, pp. 4748-4755, Jul. 2019.
[45] S. Rao, D. Wilton, and A. Glisson, "Electromagnetic scattering by surfaces of arbitrary shape," *IEEE Trans, Antennas Propag.*, vol. 30, no. 3, pp. 409-418, May 1982.
[46] W. C. Chew and J. M. Song, "Gedanken experiments to understand the internal resonance problems of electromagnetic scattering," Electromagnetics, vol. 27, no. 8, pp. 457-471, Nov. 2007.
[47] A. J. Poggio and E. K. Miller, "Integral equation solutions of threedimensional scattering problems," in *Computer Techniques for Electromagnetics* (International Series of Monographs in Electrical Engineering), R. Mittra, Ed. New York, NY, USA: Pergamon, 1973, ch. 4, pp. 159–264.
[48] Y. Chang and R. F. Harrington, "A surface formulation for characteristic modes of material bodies," *IEEE Trans. Antennas Propag.*, vol. 25, no. 6, pp. 789–795, Nov. 1977.
[49] T.-K. Wu and L. L. Tsai, "Scattering from arbitrarily-shaped lossy dielectric bodies of revolution," *Radio Sci.*, vol. 12, no. 5, pp. 709–718, Sep. 1977.
[50] J. Gu, Z. He, H. Yin, and R. S. Chen, "Fast computation of electromagnetic scattering from a metal–dielectric composite and randomly distributed BoRs cluster," *IEEE Trans. Antennas Propag.*, vol. 67, no. 12, pp. 7655-7660, Nov. 2019.
[51] T. Su, D. Z. Ding, Z. H. Fan, R. S. Chen, "Efficient analysis of EM scattering from bodies of revolution via the ACA," *IEEE Trans. Antennas Propag.*, vol. 62, no. 2, pp. 983-985, Nov. 2013.
[52] *FEKO User Manual, Suite 6.1*. Stellenbosch, South Africa: EM Softw. Syst. S.A. (Pty) Ltd., 2011
[53] H. Shao and J. Hu, ''Analysis of connected structures using equivalence principle algorithm with source reconstruction method,'' *J. Electromagn. Waves Appl*., vol. 30, no. 13, pp. 1740–1754, Sep. 2016.
[54] T. Su 1, J. Chen, J. Wang, and Y. Hu, "An improved domain decomposition algorithm for modeling dense distribution of bodies of revolution," *IEEE Access*, vol. 8, pp. 15360- 15368, 2020
[55] M. Li, M. A. Francavilla, R. S. Chen, and G. Vecchi, "Nested equivalent source approximation for the modeling of penetrable bodies," *IEEE Trans. Antennas Propag*., vol. 65, no. 2, pp. 954-959, Feb. 2017